J. Fluid Mech. (2010), *vol.* 657, *pp.* 227–237.
doi:10.1017/S0022112010002508

Negatively buoyant projectiles – from weak fountains to heavy vortices

O. J. MYRTROEEN AND G. R. HUNT†

Department of Civil and Environmental Engineering, Imperial College London, London SW7 2AZ, UK

(Received 4 February 2010; revised 22 April 2010; accepted 23 April 2010;
first published online 1 July 2010)

An experimental investigation to establish the maximum rise height z_m attained by a finite volume of fluid forced impulsively vertically upwards against its buoyancy into quiescent surroundings of uniform density is described. In the absence of a density contrast, the release propagates as a vortex ring and the vertical trajectory is limited by viscous effects. On increasing the source density of the release, gravitational effects limit the trajectory and a maximum rise height z_m is reached. For these negatively buoyant releases, the dependence of z_m on the length L of the column of ejected fluid, nozzle diameter D $(= 2r_0)$, dispensing time and source reduced gravity is determined by injecting saline solution into a fresh-water environment. For $3.4 \lesssim L/D \lesssim 9.0$, z_m/r_0 is shown to scale on the source parameter $\eta = Fr(L/D)$, a product of the source Froude number Fr and the aspect ratio L/D for the finite-volume release. Our results show that the morphology of the cap that develops above the source and the vortical motion induced within are sensitively dependent on the source conditions. Moreover, three rise-height regimes are identified: 'weak-fountain-transition', 'vorticity-development' and 'forced-release' regimes, each with a distinct morphology and dependence of dimensionless rise height on η.

Key words: plumes/thermals, vortex dynamics

1. Introduction

We consider the maximum rise height z_m attained by a volume V of miscible fluid, of source density ρ, forced vertically upwards over a time interval $0 \leqslant t \leqslant t_d$, against its buoyancy, into a still environment of uniform density $\rho_a < \rho$. In contrast to continuous releases of dense fluid, the maximum rise height and morphology of a finite volume of dense fluid released in a finite dispensing time t_d have not been considered previously.

Continuous high-Reynolds-number-fluid releases give rise to turbulent fountains (Turner 1966). A starting fountain (Marugán-Cruz, Rodríguez-Rodríguez & Martínez-Bazán 2009) entrains ambient fluid as it rises and the local momentum flux, induced by the action of the negative buoyancy, increases with height, thereby reducing the rise velocity until a maximum rise height is attained at a height $z = z_m$ above the source at $z = 0$. An exchange of momentum flux between the upflowing core and the subsequently downflowing perimeter causes the initial maximum rise height to reduce to a quasi-steady rise height. The dependence of the fountain's rise height on the fountain source Froude number Fr_0 (see (2.2)) has received considerable attention,

† Email address for correspondence: gary.hunt@imperial.ac.uk

both theoretically and experimentally (Turner 1966; Baines, Turner & Campbell 1990; Zhang & Baddour 1998; Bloomfield & Kerr 2000). The anatomy of the fountain is sensitive to Fr_0 and very weak, weak and forced-fountain regimes, each with a different rise height dependence on Fr_0, have been identified (Lin & Armfield 2000; Kaye & Hunt 2006). Low-Reynolds-number continuous releases producing laminar fountains have been examined in the work of Williamson *et al.* (2008).

The dynamics of a fountain are in stark contrast to those of injections resulting from a non-continuous (discrete) release, i.e. as established when fluid is released over a finite time interval. Impulsively releasing a cylindrical body of neutrally buoyant fluid ($\rho = \rho_a$) of length L and diameter D ($=2r_0$) into still surroundings induces a vortex ring; see Shariff & Leonard (1992) for a review. Gharib, Rambod & Shariff (1998) examined the generation and propagation of such vortex rings and established that a maximum vorticity is attained in the ring for an aspect ratio of $L/D \approx 4$. Increasing L/D beyond this value, referred to as the formation number, caused the formation of secondary vortices rather than enhancing the vorticity of the primary vortex ring.

We expect the dynamics of a finite-volume release of negatively buoyant fluid ($\rho > \rho_a$) that is forced impulsively upwards to share similarities with both a fountain and a vortex ring depending upon the dispensing time t_d, reduced gravity $g' = g(\rho - \rho_a)/\rho_a$ and volume released. For example, if t_d exceeds the time taken to reach the maximum rise height t_m, we anticipate the behaviour to be fountain-like, i.e. for fluid to attain maximum rise height and then maintain a quasi-steady height whilst fluid is being released. Conversely, for shorter dispensing times ($t_d \ll t_m$), we expect the release to be projected above the source, to reach a maximum rise height z_m whilst continuously collapsing under gravity and to potentially behave like a starting fountain for the bulk of the dispense period. The maximum rise height would increase on decreasing g' and in the limit of zero density difference ($g' = 0$) a vortex ring would propagate away from the source until all its vorticity had transferred to its wake – the nature of the ring developed depending then only on L/D (Shariff & Leonard 1992; Gharib *et al.* 1998). This contrast between fountain- and vortex-like behaviours raises the question of which source parameters govern the dynamics of negatively buoyant, or so-called heavy finite-volume releases and, for given source conditions, the extent of the vertical projection.

We report on experimental measurements and flow visualizations (§ 2) that show how the morphology of a 'cap' of dense fluid, which forms above the source during release, and a 'stem', which connects the cap to the source, change as the release propagates. We show (§ 3) that the rise height of a finite-volume release with $g' > 0$ can be characterized in terms of a source Froude number Fr and the aspect ratio of the release. Moreover, we show that for $3.4 \lesssim L/D \lesssim 9.0$ the dimensionless rise heights z_m/r_0 scale on the dimensionless source parameter $\eta = Fr \times (L/D)$. Additionally, we describe how the behaviour of a general release falls into three broad categories, namely, either a weak-fountain transitional regime, a vorticity-development regime or a forced-release regime.

2. Experiments

The releases studied were produced using a gear pump (an ISMATEC MCP-Z Process) to dispense saline solution from a smooth bore cylindrical tube (hereinafter referred to as the nozzle) into fresh water. The nozzle, with exit facing vertically upwards, was attached rigidly 15 cm above the base of a glass-sided visualization

Set	V (cm^3)	D (cm)	g' (cm s^{-2})	L/D	Symbol
1	10.0	2.15	4.50	1.29	×
2	15.0	2.15	7.37	1.94	◁
3	20.0	2.15	4.50	2.58	▷
4	25.0	2.15	7.37	3.23	✡
5	15.0	1.78	6.39	3.40	◀
6	15.0	1.78	7.37	3.40	◇
7	30.5	2.15	4.39	3.93	□
8	35.0	2.15	4.50	4.52	○
9	40.0	2.15	4.50	5.16	*
10	40.0	2.15	7.37	5.16	△
11	20.0	1.70	4.50	5.18	▽
12	25.0	1.78	7.37	5.66	+
13	40.0	1.78	6.39	9.06	▶
14	40.0	1.78	7.37	9.06	•

TABLE 1. Summary of release conditions.

tank. The tank, of plan area 176 cm × 125 cm, was filled with water to a depth of 100 cm. Saline solution was fed to the pump from a 20 l reservoir which was immersed in the tank in order to equalize temperatures between the source fluid and the release environment. The densities of the source and ambient fluids were measured using an Anton PAAR DMA 4500 densitometer ($\pm 5 \times 10^{-5}$ g cm^{-3}). The tank was uniformly backlit using a light box containing an array of high-frequency fluorescent tubes and visualization of the release dynamics was achieved by infusing the saline solution with methylene blue of approximate concentration 0.1 mg cm^{-3}. Images of the flow were captured using a JAI CVM4$^+$CL camera with a Pentax 12.5–75 mm 1:1.8 TV ZOOM lens and a Hoya R(25A) filter. The camera was connected to a computer-controlled BitFlow R3 frame grabber card and Matlab R2007a was used to process the captured images.

The gear pump settings, namely the number of revolutions per minute (r.p.m.) and the dispensing time t_d, could be varied independently. This allowed, for example, a constant volume V to be ejected over a range of dispensing times. A high r.p.m. in combination with a small t_d produced 'highly forced' releases, whilst a low r.p.m. in combination with a large t_d produced 'weakly forced' releases. Volumes of 10 ± 0.1 cm$^3 \leqslant V \leqslant 40 \pm 0.4$ cm^3 with reduced gravities 4 cm s$^{-2} \leqslant g' \leqslant 7$ cm s^{-2} were dispensed over times $0.16 \pm 0.002\,\text{s} \leqslant t_d \leqslant 6.92 \pm 0.07\,\text{s}$. Measurements of the exit-velocity history (achieved by tracking a front in a clear acrylic nozzle at 24 Hz) indicated a period of constant exit velocity w for a duration t_d and a subsequent period of linearly decreasing velocity of duration $0.2t_d$. Three nozzles, of diameters $D = 2.15$, 1.78 and 1.70 cm, enabled releases of aspect ratios $1.29 \leqslant L/D \leqslant 9.06$. The overall length of each nozzle (30 cm) exceeded the longest ejected column of saline solution ($L = 16.1$ cm), so that the fluid was ejected solely from the nozzle and not from the adjoining rigid tubing. Release conditions are given in table 1.

The saline releases were of high Péclet number ($Pe \sim O(10^8)$) so that diffusive effects over the time scale of the developing flow were small (typically $t_m \lesssim 10$ s), and of relatively high exit Reynolds number ($Re \sim O(10^3)$). Dimensional considerations then indicate that the dimensionless groups L/D and Fr (see (2.1)) govern the behaviour of a finite-volume negatively buoyant release. The Froude number Fr, for the finite-volume release, may be established from a physical viewpoint

by considering the ratio of the dominant forces acting upon the release – the impulsive vertical force that ejects fluid from the nozzle into the quiescent surroundings ($\rho V w/t_d$) and the buoyancy force ($\rho_a g' V$):

$$Fr = \left(\frac{\rho V w/t_d}{\rho_a g' V}\right)^{1/2} = \sqrt{\frac{w}{g' t_d}}\sqrt{\frac{\rho}{\rho_a}} = \frac{w}{\sqrt{g' L}}\sqrt{\frac{\rho}{\rho_a}}. \tag{2.1}$$

For a continuous release giving rise to a fountain,

$$Fr_0 = w/\sqrt{g' D/2}. \tag{2.2}$$

Restricting our attention to the Boussinesq case as $\rho/\rho_a \approx 1$ for the small-density differences considered herein, $Fr_0/Fr \propto \sqrt{L/D}$ and $Fr = w/\sqrt{g' L}$. This indicates that it is the dependence on the aspect ratio L/D that distinguishes the source conditions of finite-volume releases dispensed over finite times from releases producing continuous fountains. The parameter space explored in our experiments was limited by the apparatus to a maximum forcing equivalent of $Fr_0 \approx 6$ and $L/D \approx 9$. Fourteen sets of experiments were run to establish the dependence of the rise height and release morphology on these parameters. Over 300 individual experiments were performed in total.

3. Results and discussion

Figure 1 shows the development of eight releases (r1–r8) of identical g', L and D, with successively decreasing dispensing times t_d, as they approach maximum rise height at a time $t/t_m = 1$. Each row of seven still images captures the release at the normalized times $t/t_m = \{0.25, 0.38, 0.50, 0.63, 0.75, 0.88, 1.00\}$. To enable direct comparison between the shape and size of the individual releases, the images are of identical scale. The vertical extent of the grey surrounding frame in row 8 corresponds to 15 cm (image resolution 1170 vertical $\times$ 826 horizontal pixels). It is clear that the release dynamics are sensitively dependent upon the dispensing time t_d. This is apparent on viewing column 7, which shows the strikingly different forms of the releases at their maximum rise height. Moreover, a change in the initial development of the releases with t_d is also apparent (on viewing column 1). Reducing t_d by approximately a factor of 4 (r1–r8) increases the rise height by approximately a factor of 8 (from $z_m/r_0 = 1.65$ to 13.8), and the shape of the release and its dynamics are altered completely.

It is evident then that the ratio of the time taken to reach maximum height t_m (not known *a priori*) and the time to dispense t_d influences the anatomy of a release. For $t_d \geqslant t_m$, as in r1, fluid released reached a maximum rise height before dispensing finished. Here, the release appears and behaves like a weak fountain as achieved by a continuous release (cf. Kaye & Hunt 2006) and the rise heights scale accordingly (figure 2*b*). For these releases the value of L/D did not influence rise height. As t_d decreased, so that $t_d < t_m$, the rise height increased and the release morphology changed from a shape resembling an oblate hemisphere, with weak-fountain-like behaviour, to a mushroom-shaped structure; compare releases r1–r4. For the latter, a distinct 'cap' formed that connected to the source via a 'stem' or conduit of fluid whose radius typically decreased to a neck immediately above the nozzle.

A build-up of vorticity was observed within the cap as it formed. The contained vortical motion became increasingly distinct as t_d decreased and discernible as sharp lines of circulation (e.g. r5 and r6). During the very early transients the short stem acted as a conduit channelling fluid up to the developing cap (e.g. r6 for $t/t_m = 0.25$).

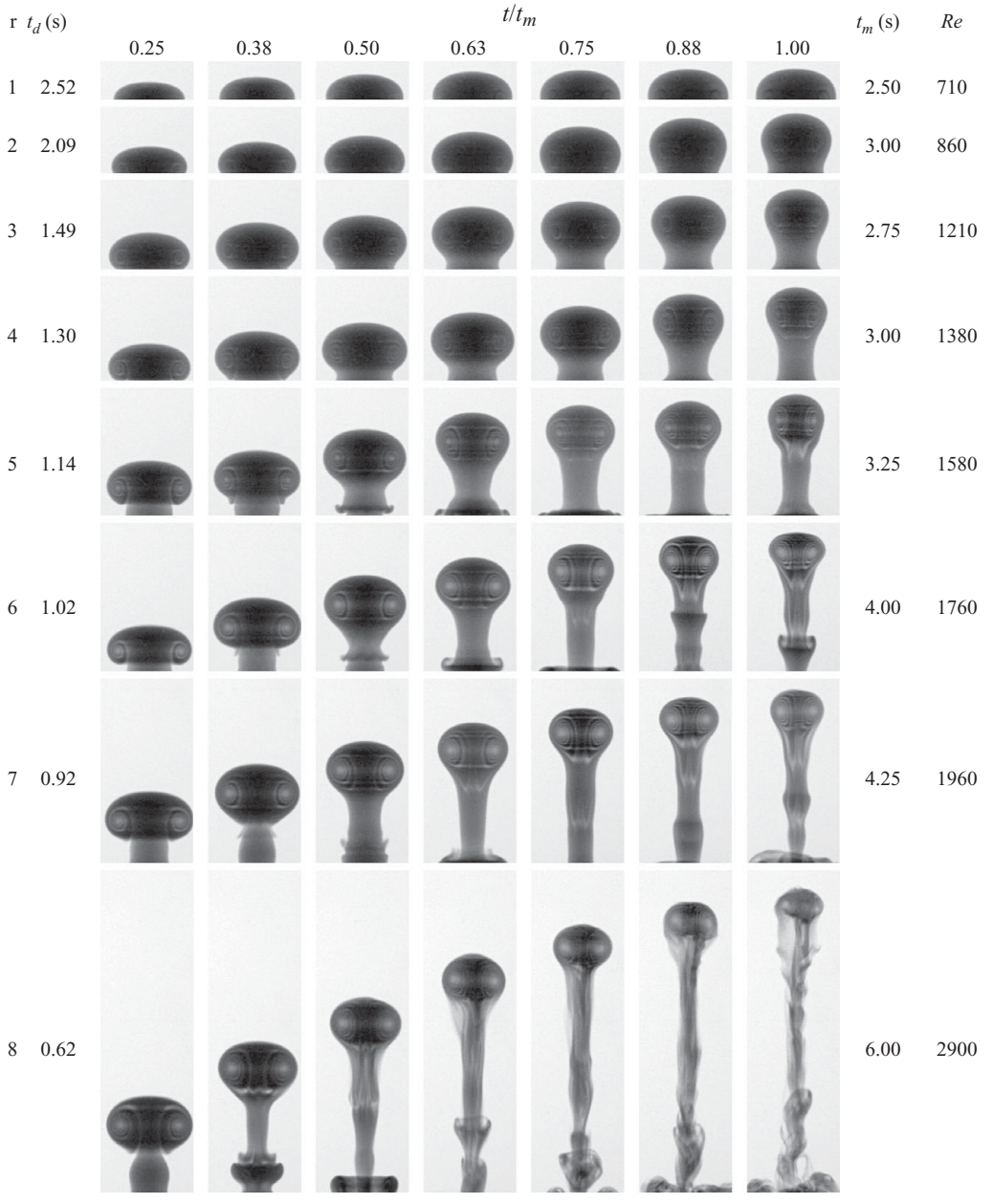

FIGURE 1. Images of eight releases (r1–r8) from a time $t/t_m = 0.25$ to the time of maximum rise height $t/t_m = 1.00$. The images show the effects of increased source forcing on the rise height and flow structure as achieved by successively reducing the dispensing time t_d for $L/D = 3.93$, $V = 30.5$ cm^3, $D = 2.15$ cm and $g' = 4.39$ cm s^{-2} so that $Fr_0 = 3.89/t_d$, producing 1.5 (row 1) $< Fr_0 < 6.3$ (row 8). $Re = wD/\nu$, where $\nu = 10^{-2}$ cm^2 s^{-1}.

At later times, e.g. when dispensing was complete, the direction of flow was reversed in the stem and dense fluid descended under gravity from the cap back towards the source. The outline perimeter of the flow became reminiscent of a pipette, i.e. with an elliptical cap atop a column of the descending fluid with decreasing diameter (e.g. r7 at

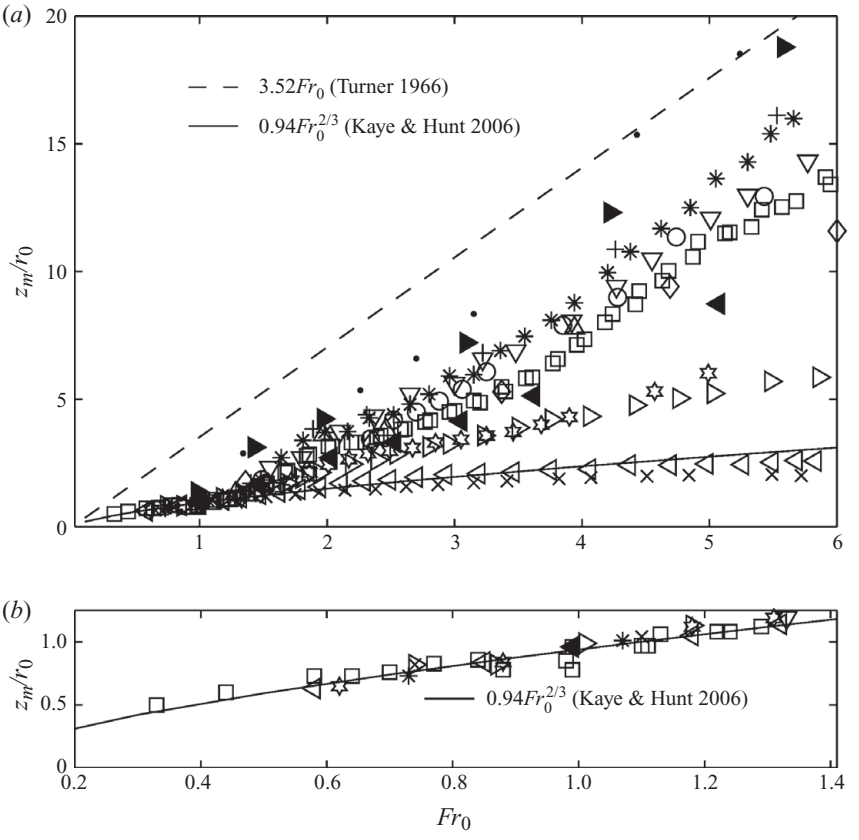

FIGURE 2. Dimensionless rise heights. (*a*) z_m/r_0 versus Fr_0, showing the variation with L/D. (*b*) Exploded view of (*a*) for $0.2 < Fr_0 < 1.4$. Also plotted are rise heights for 'very weak' fountains (—) and for 'highly-forced' fountains (- - -). For an explanation of the symbols in this and subsequent figures, see table 1.

$t/t_m = 0.63$). Instabilities were triggered (e.g. r6 for $t/t_m = \{0.88, 1\}$) and appeared on curtains of fluid flowing down around the stem's perimeter. For $t_d \ll t_m$, the rise height was sufficiently large that the axisymmetry of the descending flow, which consisted of fluid which had drained from the cap, was broken. This is particularly clear in r8 for $t/t_m = 0.88$ and 1. The volume of the vortex cap initially increased to a maximum and visibly decreased during its subsequent rise as a consequence of the descending fluid (compare r6 at $t/t_m = 0.50$ with $t/t_m = 1.00$). The draining of the fluid from the vortex is clearly pronounced for r7 and r8 which show marked reductions in cap volumes as maximum rise height is approached.

Releases for which $t_d \gg t_m$ gave rise to fountains, whose rise heights may be classified solely in terms of Fr_0. For truly continuous releases, the rise height scaled on the source radius has been shown to collapse onto a single curve when plotted against Fr_0; see Turner (1966) and data collated from a number of authors in Kaye & Hunt (2006). It was thus of interest to plot z_m/r_0 against Fr_0 for our discrete releases and compare directly with fountain rise heights. Figure 2 plots the dimensionless rise heights, associated with 12 aspect ratios within the range $1.29 \leqslant L/D \leqslant 9.06$, against Fr_0, which was increased for a given nozzle by reducing either g' or t_d. The rise heights for very weak fountains ($z_{ss}/r_0 = 0.94Fr_0^{2/3}$, Kaye & Hunt 2006) and forced fountains ($z_m/r_0 = 3.52Fr_0$, Turner 1966) are included for comparison.

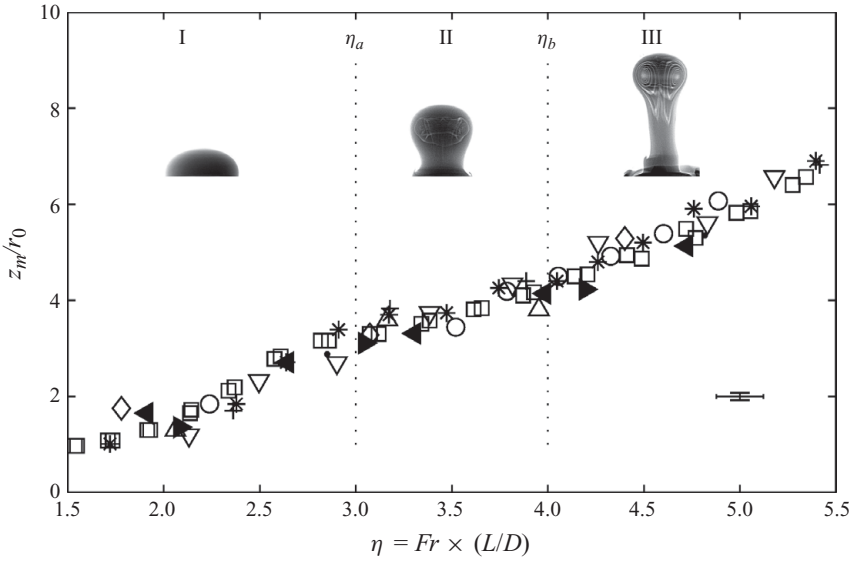

FIGURE 3. z_m/r_0 versus η showing collapse of rise-height data for $3.4 \leqslant L/D \leqslant 9.06$ (data for $L/D < 3.4$ fall below the collapsed data). (I) Weak-fountain, (II) vorticity-generation and (III) forced-release regions are demarked. Inset images depict typical flow morphology at maximum rise height. The estimated maximum experimental error is shown in the lower right corner.

For a given L/D, increasing Fr_0 increased the rise height of a discrete release (figure 2*a*), confirming the trends shown in figure 1. For $Fr_0 \lesssim 1.4$, the rise heights of the discrete releases are independent of L/D and show a close correlation with the rise-height predictions for very weak fountains (figure 2*a* for $Fr_0 \lesssim 1.4$ and figure 2*b*). The collapse of the rise-height data for $Fr_0 \lesssim 1.4$ and adherence to the weak-fountain predictions break down once the inertia force driving the release becomes sufficiently dominant relative to the opposing buoyancy force. This is evident for $Fr_0 > 1.4$ as the sets of rise-height data begin to fan out in lines of constant L/D, thereby marking the onset of a dependence on L/D. For $Fr_0 \gtrsim 1.4$, an increase in L/D results in a rise in z_m/r_0 for a given Fr_0, a rise which is increasingly prominent for higher values of Fr_0, other than for releases with weak-fountain-like behaviour. For $1 \lesssim L/D \lesssim 2$ (1.29 ($\times$), 1.94 ($\triangleleft$)) the increase in rise height with Fr_0 is weak and a $z_m/r_0 \sim Fr_0^{2/3}$ weak-fountain-like behaviour is maintained over the entire range of Fr_0 examined – and notably for Fr_0 exceeding (e.g. $Fr_0 = 6$) that for which weak-fountain behaviour is expected in a continuous release. For larger L/D a stronger variation in z_m/r_0 with Fr_0 is observed and rise-heights approach, but are bounded from above by, those attained by a 'highly-forced' fountain where $z_m/r_0 \sim Fr_0$.

Figure 3 shows the dimensionless maximum rise heights for $L/D \geqslant 3.4$ plotted against

$$\eta = Fr\frac{L}{D} = \frac{Fr_0}{\sqrt{2}}\left(\frac{L}{D}\right)^{1/2} = \frac{t_b}{t_d}\frac{L}{D}, \tag{3.1}$$

which expresses a ratio of a characteristic buoyancy time scale $t_b = \sqrt{L/g'}$ to the dispensing time t_d for the fluid volume, of aspect ratio L/D, released. The z_m/r_0 versus η scaling (figure 3) provides a very good collapse of the data, showing no systematic variation with L/D, and thus indicates that for the range of L/D examined, the rise height may be expressed solely in terms of η and it increases with increasing

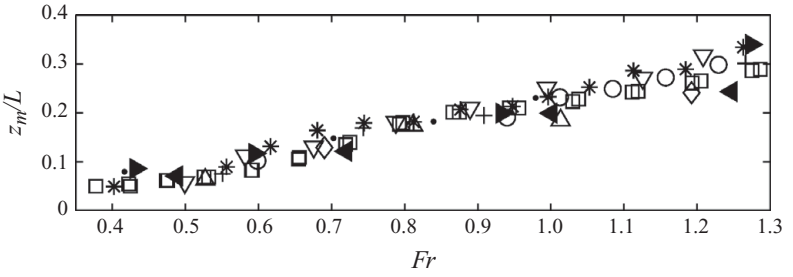

FIGURE 4. z_m/L versus Fr. Data shown for $L/D > 3.4$.

η. For η to remain constant on increasing L/D (i.e. on ejecting a greater volume from a given nozzle) and thereby to achieve a constant height of projection, it is necessary to decrease the ratio t_b/t_d. This may be achieved by either decreasing the forcing (by increasing t_d) or by increasing the buoyancy of the release. Similarly, a reduced buoyancy of release would require an increase of t_d or decrease in L/D in order to produce the same η and thus the same dimensionless vertical projection. For $L/D < 3.4$, a decrease in L/D for a constant η resulted in a reduction of z_m/r_0.

Vorticity formation in vortex rings offers an explanation as to why there is a collapse in dimensionless rise heights for $9.0 \gtrsim L/D \gtrsim 3.4$. Different approaches to model vortex ring formation (see Dabiri 2009 for a review) predict maximum vortex ring growth at a formation number, or critical aspect ratio, of $(L/D)_{cr} \approx 4$. Recent studies by Wang *et al.* (2009) and Marugán-Cruz *et al.* (2009) suggest that buoyancy influences $(L/D)_{cr}$, which may decrease with negative buoyancy. Our value of $(L/D)_{cr} = 3.4$, above which our rise-height data collapse, supports this trend.

Three regions (I, II and III) are identified and demarked on figure 3. The regions are referred to as (I) the weak-fountain, (II) the vorticity-development and (III) the forced-release regimes. The rise-height data presented in figure 3 are replotted in figure 4 after dividing both axis scales by L/D. The resulting z_m/L versus Fr scaling provides a good collapse of the data and trends similar to those in figure 3. The fact that the rise height z_m/L scales on Fr (figure 4) is unsurprising when one considers the analogous scaling for continuous fountains, the length scale for the discrete release being L for both the vertical rise and the buoyancy velocity rather than r_0 (or equivalently D) for the fountain. That said, the variation between rise-height regimes and the demarcation between them, as discussed in §§ 3.1–3.3, are clearer in figure 3. To further highlight the flow morphologies and aid the following discussion, still images taken in regimes I, II and III at the time of maximum rise height are, respectively, shown in rows 1, 2 and 3 of figure 5. The discussion of following regimes applies for $L/D \gtrsim 3.4$.

3.1. *Regime I: Weak fountain and transition*

For $Fr_0 \lesssim 1.4$ releases are dominated by their buoyancy and collapse upon dispensing, spilling over the nozzle perimeter like fluid over a weir. The releases adhere to weak-fountain rise-height predictions as z_m is attained before dispensing is complete. A good collapse of the z_m/r_0 data with Fr_0 is achieved irrespective of L/D (figure 2*b*) and thus η (see (3.1)) plays no direct role. As the effect of inertia becomes increasingly dominant there is a departure from the weak-fountain rise-height behaviour. Specifically, for $Fr_0 \gtrsim 1.4$ there is a transition, as shown in figure 5 (row 1), to the so-called vorticity-development regime (§ 3.2 and figure 5, row 2). Within this transition the variation

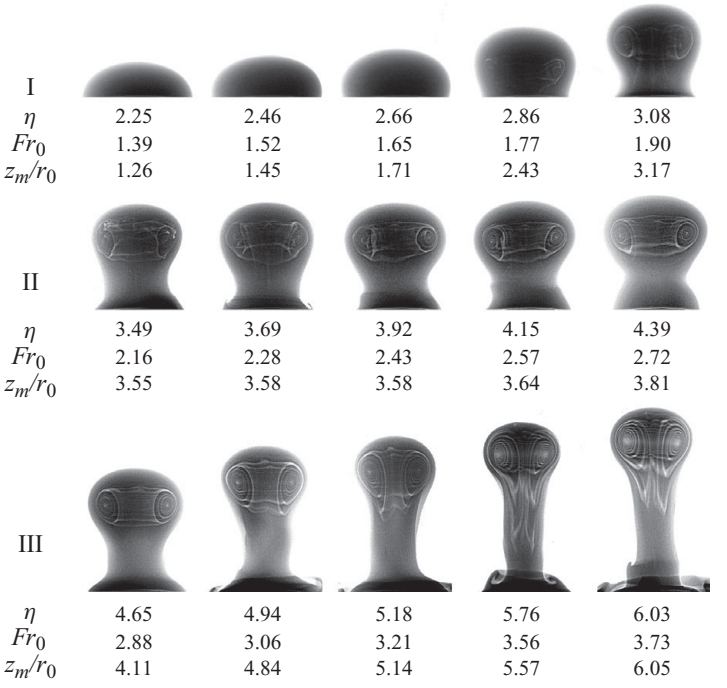

FIGURE 5. Images at maximum rise height showing releases in the (I) weak-fountain, (II) vorticity-generation and (III) forced-release regimes. For each of the 15 releases shown, $D = 2.15$ cm, $V = 40.0$ cm^3, $L/D = 5.16$ and $g' = 7.49$ cm s^{-2}. Fr_0 was increased by decreasing t_d.

of rise height with Fr_0 is stronger than for a weak fountain. Notably, the stills taken within regime I display little or no discernible vorticity (e.g. columns 2–4).

3.2. *Regime II: Vorticity development* ($\eta_a \leqslant \eta \leqslant \eta_b$, $Fr_0 \gtrsim 1.4$)

With increased forcing, vortical motions become apparent as the head of the release changes from a collapsing body of fluid to a distinct vortex cap – compare rows 1 and 2 of figure 5. In the 'vorticity-development' regime, increased forcing alters the flow within the cap but does not significantly increase the rise height. The structure within the cap develops from an unorganized flow (row 2, column 1) to a coherent and symmetrical vortex (row 2, column 5). Thus, the increase in kinetic energy input at the source as forcing increases serves primarily to raise the vorticity in the head. This can be seen for $3 \lesssim \eta \lesssim 4$ (figure 5), suggesting $\eta_a \approx 3$ and $\eta_b \approx 4$ for $L/D = 5.16$. The value $\eta = \eta_b$ corresponds to maximal vorticity in the cap and marks the upper limit of this regime.

3.3. *Regime III: Forced-release regime* ($\eta \gtrsim \eta_b$, $Fr_0 \gtrsim 1.4$)

Once the source forcing is sufficient to induce a maximal vorticity any further increase in forcing serves primarily to propel the head further from the source (figure 5, row 3). It is clear that η controls the rise heights for the range of $\{Fr_0, L/D\}$ parameter space considered (figure 3). Independently increasing Fr_0 and L/D would induce a vortex ring for sufficiently large Fr_0 (either containing all the release fluid or atop a trailing jet for $L/D \gg (L/D)_{cr}$) and a continuous fountain for $L/D \to \infty$.

Relative to fountains, where rise heights are controlled solely by Fr_0, finite-volume releases of sufficiently low L/D may be regarded as experiencing a 'lack of fluid'. This is responsible for the η dependency and prevents true fountain-like behaviour, i.e. rise heights following the dashed line in figure 2 for $Fr_0 \gg 1$. As L/D increases, this fluid deficit subsides with η_b approaching η_a. (The precise variation of η_b with L/D has yet to be determined.) For sufficiently large L/D, the rise height reverts to a dependence solely on Fr_0; there is some evidence of this in figure 2 where release rise heights coincide with forced-fountain rise-height predictions, e.g. for $L/D = 9.06$ (•, ►) at $Fr_0 \gtrsim 4.4$. Marugán-Cruz *et al.* (2009) show that vorticity establishment in the cap of a starting fountain, i.e. a release with no deficit of fluid ($L/D \to \infty$), occurs at $Fr_0 \approx 1.4$. Given that vorticity development in finite-volume releases occurs at $\eta_a \approx 3$, from (3.1) $Fr_0 \gtrsim 1.4$ requires $L/D \gtrsim 9$. In other words, $L/D \gtrsim 9$ may be regarded as a sufficient supply of fluid to enable rise-height behaviour seen in continuous fountains.

4. Conclusions

We have described an experimental investigation concerning a finite-volume release of dense fluid forced vertically upwards, against its buoyancy, into still and uniform surroundings. The rise heights and morphologies of these releases were examined for injections of saline solution into fresh water. Our results demonstrate that the maximum rise heights are governed by the release aspect ratio L/D and a source Froude number Fr based on the length of the fluid cylinder ejected.

The maximum rise-height data z_m/r_0 collapsed when plotted against $Fr(L/D)$ for $(L/D)_{cr} \lesssim L/D \lesssim 9.0$, where $(L/D)_{cr} \approx 3.4$, and additionally for z_m/L plotted directly against Fr. For $L/D < (L/D)_{cr}$ the vorticity within the release is below maximum and thus the rise height attained on subsequently increasing L/D may be regarded as being limited by vorticity development. For the range of Fr considered, the collapse of the rise-height data when plotted as z_m/L versus Fr is more readily interpreted in that the dominant length scale is the physical length of the release rather than the source diameter as for continuous releases producing fountains. For $(L/D)_{cr} \lesssim L/D \lesssim 9.0$, the variation of dimensionless rise height with source conditions and the shape and internal structure of the flow allowed the releases to be classified into three regimes: (I) 'weak-fountain' transition, characterized solely by Fr_0 provided $Fr_0 \lesssim 1.4$; (II) 'vorticity-development', where rise heights are limited by a 'lack of fluid' and increased forcing primarily generates vorticity in the head and (III) forced-release behaviour, where the vorticity in the head is fully established and increased forcing projects the release further. The maximum rise heights were bounded by the maximum rise height of a forced fountain from above and a weak fountain from below. Due to limitations of our apparatus, the vertical projection of releases for $Fr > 1.3$ ($Fr_0 > 6$) was not possible but would be of future interest, as would examining releases for $L/D < 1$.

The authors gratefully acknowledge funding from Imperial College's Urban Cities Programme and comments from an anonymous referee and Professor Paul F. Linden on an earlier draft.

REFERENCES

Baines, W. D., Turner, J. S. & Campbell, I. H. 1990 Turbulent fountains in an open chamber. *J. Fluid Mech.* **212**, 557–592.

Bloomfield, L. J. & Kerr, R. C. 2000 A theoretical model of a turbulent fountain. *J. Fluid Mech.* **424**, 197–216.

Dabiri, J. O. 2009 Optimal vortex formation as a unifying principle in biological propulsion. *Annu. Rev. Fluid Mech.* **41**, 17–33.

Gharib, M., Rambod, E. & Shariff, K. 1998 A universal time scale for vortex ring formation. *J. Fluid Mech.* **360**, 121–140.

Kaye, N. B. & Hunt, G. R. 2006 Weak fountains. *J. Fluid Mech.* **558**, 319–328.

Lin, W. & Armfield, S. W. 2000 Very weak fountains in a homogeneous fluid. *Numer. Heat Transfer* A **38**, 377–396.

Marugán-Cruz, C., Rodríguez-Rodríguez, J. & Martínez-Bazán, C. 2009 Negatively buoyant starting jets. *Phys. Fluids* **21**, 117101.

Shariff, K. & Leonard, A. 1992 Vortex rings. *Annu. Rev. Fluid Mech.* **24**, 235–279.

Turner, J. S. 1966 Jets and plumes with negative or reversing buoyancy. *J. Fluid Mech.* **26**, 779–792.

Wang, R. Q., Law, A. W. K., Adams, E. E. & Fringer, O. B. 2009 Buoyant formation number of a starting buoyant jet. *Phys. Fluids* **21** (12), 125104.

Williamson, N., Srinarayana, N., Armfield, S. W., McBain, G. D. & Lin, W. 2008 Low-Reynolds-number fountain behaviour. *J. Fluid Mech.* **608**, 297–317.

Zhang, H. & Baddour, R. E. 1998 Maximum penetration of vertical round dense jets at small and large Froude numbers. *J. Hydraul. Engng* **124**, 550–553.